Science Advances
AAAS

Supplementary Materials for

Structure-guided design enables development of a hyperpolarized molecular probe for the detection of aminopeptidase N activity in vivo

Yutaro Saito, Hiroyuki Yatabe, Iori Tamura, Yohei Kondo, Ryo Ishida, Tomohiro Seki, Keita Hiraga, Akihiro Eguchi, Yoichi Takakusagi, Keisuke Saito, Nobu Oshima, Hiroshi Ishikita, Kazutoshi Yamamoto, Murali C. Krishna*, Shinsuke Sando*

*Corresponding author. Email: cherukum@mail.nih.gov (M.C.K.); ssando@chembio.t.u-tokyo.ac.jp (S.S.)

Published 30 March 2022, *Sci. Adv.* **8**, eabj2667 (2022)
DOI: 10.1126/sciadv.abj2667

The PDF file includes:

Other Supplementary Material for this manuscript includes the following:

1. Binding energy calculations

As stated in Fig. 2, the calculated binding energies are similar for the substrates (Ala-NH_2, Ala-Gly, and Ala-Gly-NMe_2) when Glu384 is deprotonated and the hydrogen-bond is absent (fig. S1).

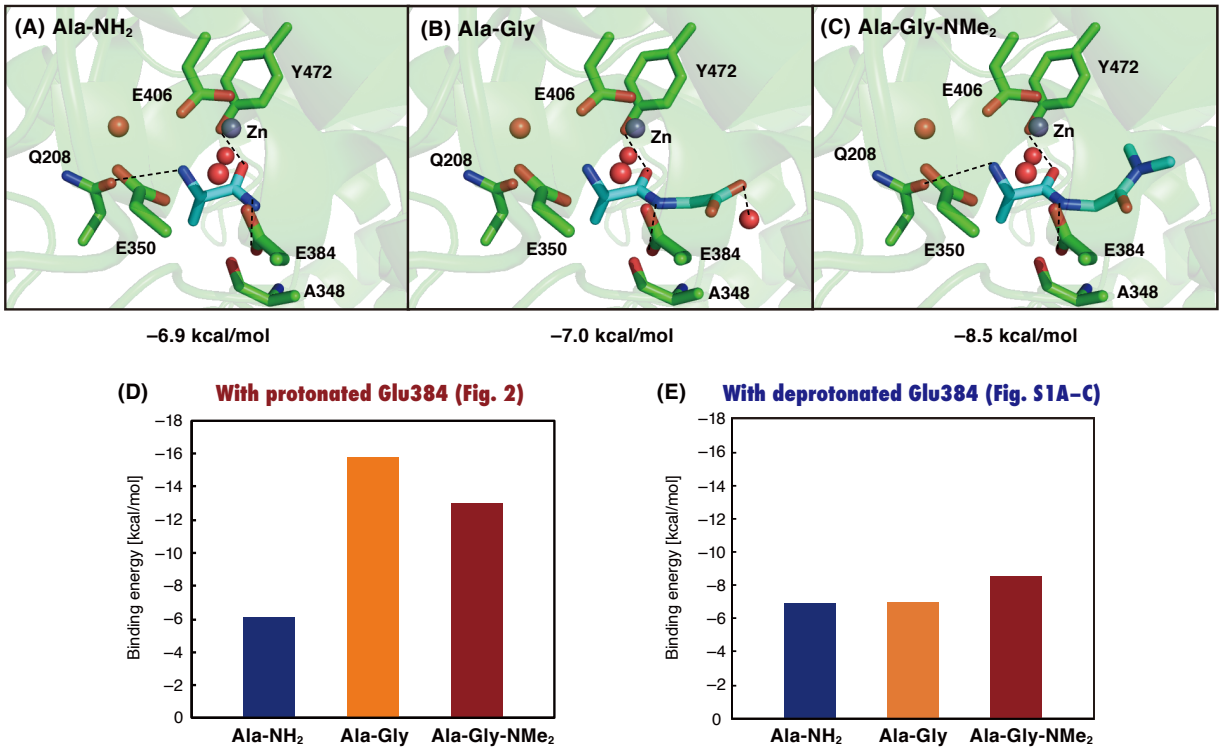

Fig. S1. Substrate binding sites and binding energies when Glu384 is protonated (Fig. 2) or deprotonated.

(**A**–**C**) QM/MM-optimized geometries and calculated substrate-APN binding energies of (**A**) Ala-NH_2-APN, (**B**) Ala-Gly-APN, and (**C**) Ala-Gly-NMe_2-APN when Glu384 is deprotonated. Red balls indicate water molecules. Dashed lines indicate electrostatic interactions. The calculated binding energies are described below the figures. (**D**, **E**) Bar graphs of the calculated binding energies when Glu384 is (**D**) protonated or (**E**) deprotonated.

2. T_1 relaxation analysis (34)

Theoretically, T_1 relaxation is decomposed to each relaxation mechanism according to the following eq. 1.

$$\frac{1}{T_1{}^{tot}} = \frac{1}{T_1{}^{DD}} + \frac{1}{T_1{}^{CSA}} + \frac{1}{T_1{}^{O_2}} + \frac{1}{T_1{}^{res}} \qquad (eq.1)$$

Here, inversion of each T_1 contribution is expressed as $R_1{}^{X}$, as shown in eq. 2

$$R_1{}^{tot} = R_1{}^{DD} + R_1{}^{CSA} + R_1{}^{O_2} + R_1{}^{res} \qquad (eq.2)$$

where $R_1{}^{tot}$ is total of T_1 relaxation components; $R_1{}^{DD}$ is T_1 relaxation by dipole–dipole interaction, here we especially focus on dipole–dipole interaction between ^{13}C and ^{1}H nuclei that mainly contributes to the relaxation; $R_1{}^{CSA}$ is T_1 relaxation of chemical shift anisotropy; $R_1{}^{O_2}$ is T_1 relaxation by dipole–dipole interaction between ^{13}C and O_2 molecules existing in the solvent; $R_1{}^{res}$ is residual factors including spin rotation and scalar coupling (35). In this paper, $R_1{}^{DD}$ and $R_1{}^{O_2}$ for each and $R_1{}^{CSA}$ for Ala-[1-^{13}C]Gly-d_2-NMe$_2$ at 9.4 T were determined according to the reported procedure (34). The result is shown in fig. S2. The further information for $R_1{}^{CSA}$ is shown in fig. S13.

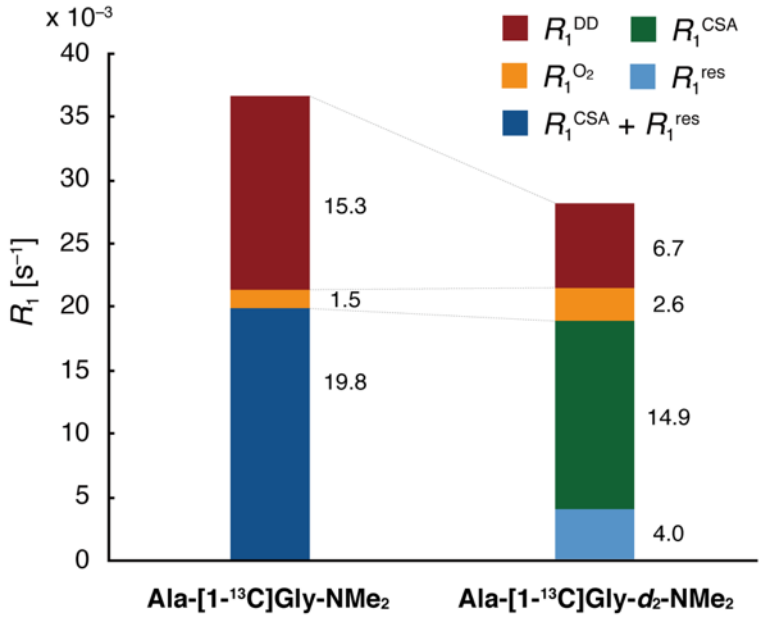

Fig. S2. T_1 relaxation analysis of Ala-[1-^{13}C]Gly-NMe$_2$ and Ala-[1-^{13}C]Gly-d_2-NMe$_2$ at 9.4 T.

3. Synthetic scheme of Ala-[1-^{13}C]Gly-d_2-NMe$_2$

Synthesis of Ala-[1-^{13}C]Gly-d_2-NMe$_2$ used in Figs. 3, 5C and 6 (91% deuterated efficiency) was performed according to fig. S3. This synthetic scheme can be applied to the gram-scale synthesis. The amount of obtained Ala-[1-^{13}C]Gly-d_2-NMe$_2$ was 1.45 g. The total yield from [1-^{13}C]Gly (1.00 g, 13.1 mmol) was 63% with 91% deuterated efficiency at α-position of Gly-moiety. See the Materials and Methods section for the detailed procedure.

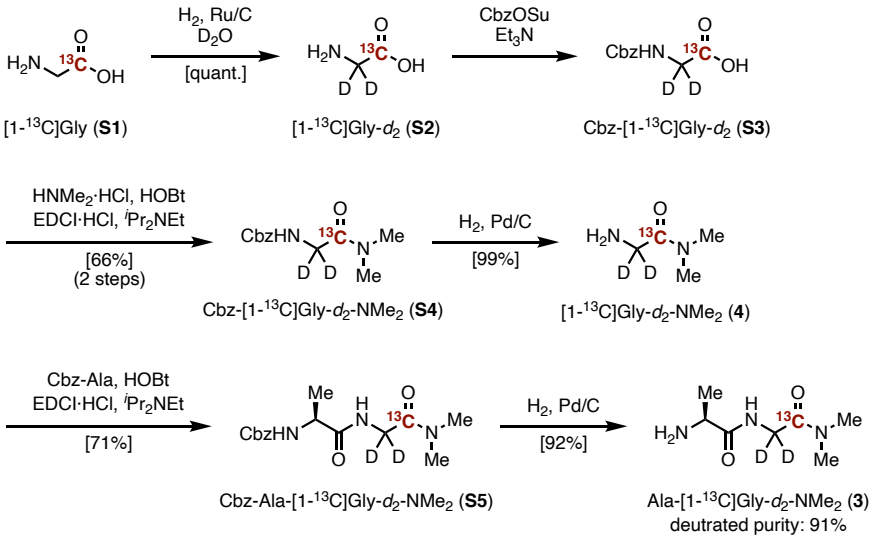

Fig. S3. Synthetic route for Ala-[1-^{13}C]Gly-d_2-NMe$_2$.

In an early stage of this study, different protocol was employed for deuteration and Cbz-protection steps of glycine (fig. S4). Through this scheme, Ala-[1-^{13}C]Gly-d_2-NMe$_2$ was obtained in 33% total yield with 83% deuterated efficiency at α-position of Gly-moiety. This sample was used for the experiments shown in Fig. 5D.

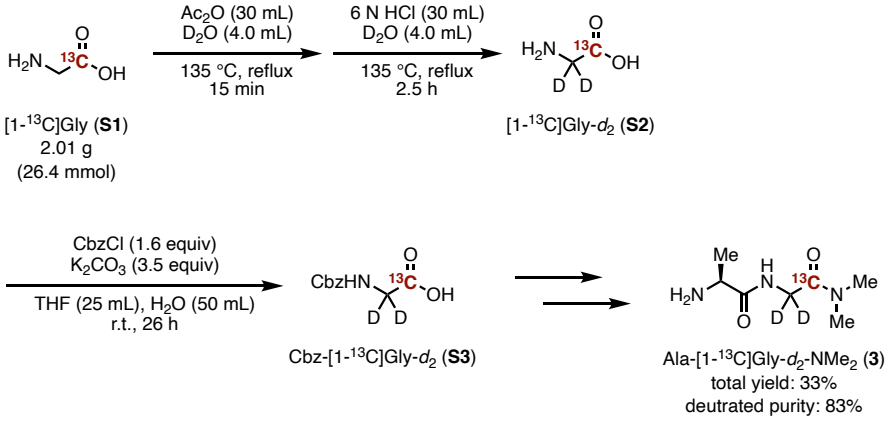

Fig. S4. Another synthetic route for Ala-[1-^{13}C]Gly-d_2-NMe$_2$.

4. *In vitro* experiment under thermal equilibrium state

Detection of APN-activity using Ala-[1-^{13}C]Gly-d_2-NMe$_2$ under thermal equilibrium state

Figs. S5 and S6 are the whole spectra (x-offset: –25 ppm to 225 ppm) of the thermally equilibrated ^{13}C NMR spectra shown in Fig. 5B. No peak except ones of Ala-[1-^{13}C]Gly-d_2-NMe$_2$, [1-^{13}C]Gly-d_2-NMe$_2$, and DMSO (an internal standard) was observed. The detailed procedure is described in Materials and Methods section.

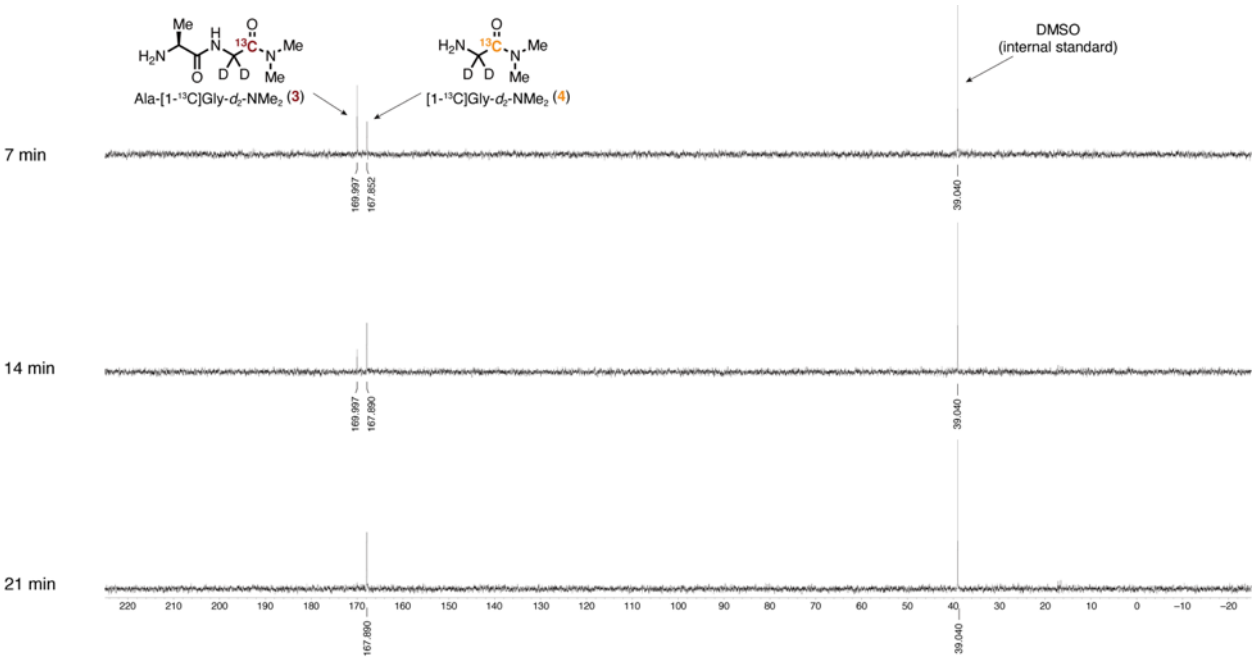

Fig. S5. Thermally equilibrated ^{13}C NMR spectra of Ala-[1-^{13}C]Gly-d_2-NMe$_2$ incubated in mouse kidney homogenate.

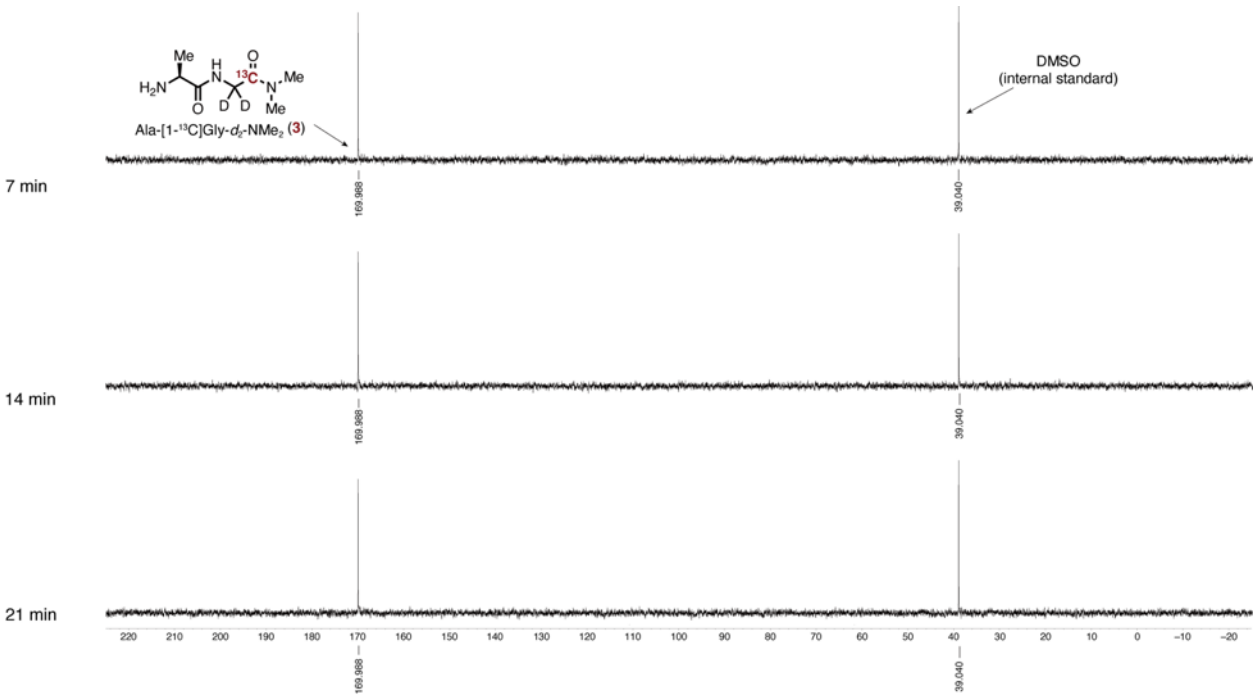

Fig. S6. Thermally equilibrated ^{13}C NMR spectra of Ala-[1-^{13}C]Gly-d_2-NMe$_2$ incubated in mouse kidney homogenate, in the presence of phebestin as an APN-inhibitor.

Figs. S7 and S8 show the thermally equilibrated ^{13}C NMR spectra of Ala-[1-^{13}C]Gly-d_2-NMe_2 incubated in homogenate of mouse tumor xenograft (MIA PaCa-2) in the presence or the absence of phebestin, an APN inhibitor. In these experiments, it was confirmed that the same reaction with that in kidney homogenate (shown in Fig. 5B and figs. S5 and S6) occurred although the conversion of Ala-[1-^{13}C]Gly-d_2-NMe_2 was slower than that in Fig. 5B and fig. S5.

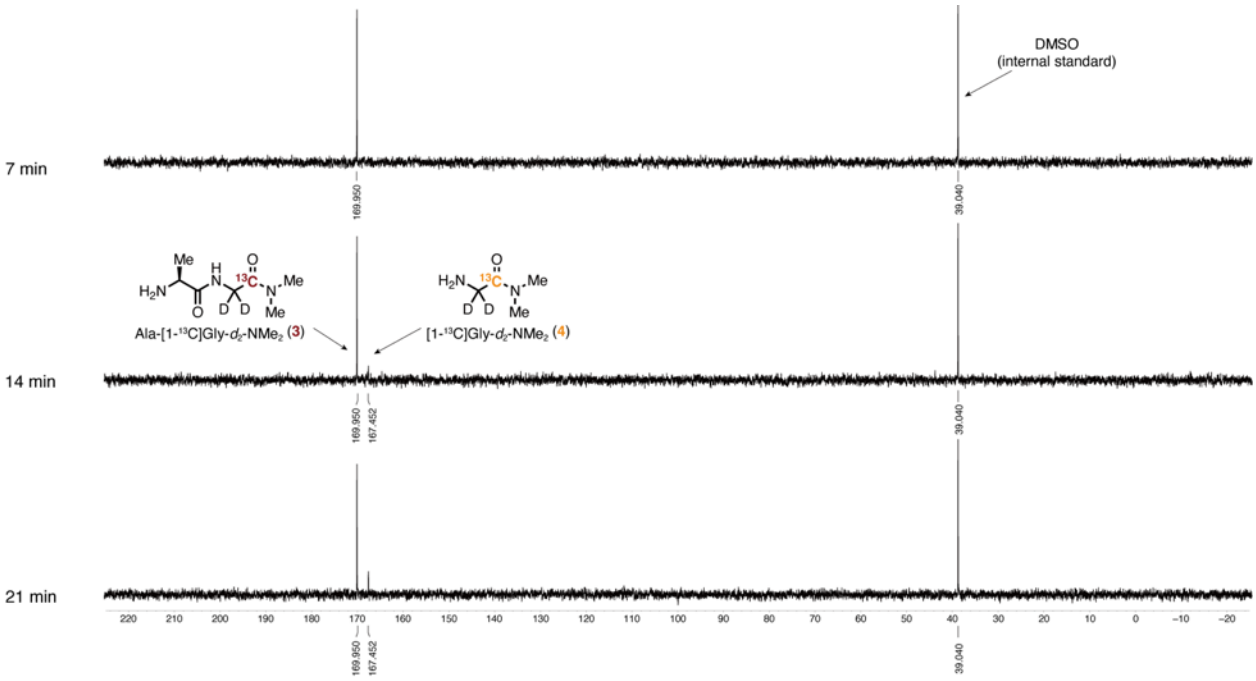

Fig. S7. Thermally equilibrated ^{13}C NMR spectra of Ala-[1-^{13}C]Gly-d_2-NMe_2 incubated in homogenate of mouse tumor xenograft (MIA PaCa-2).

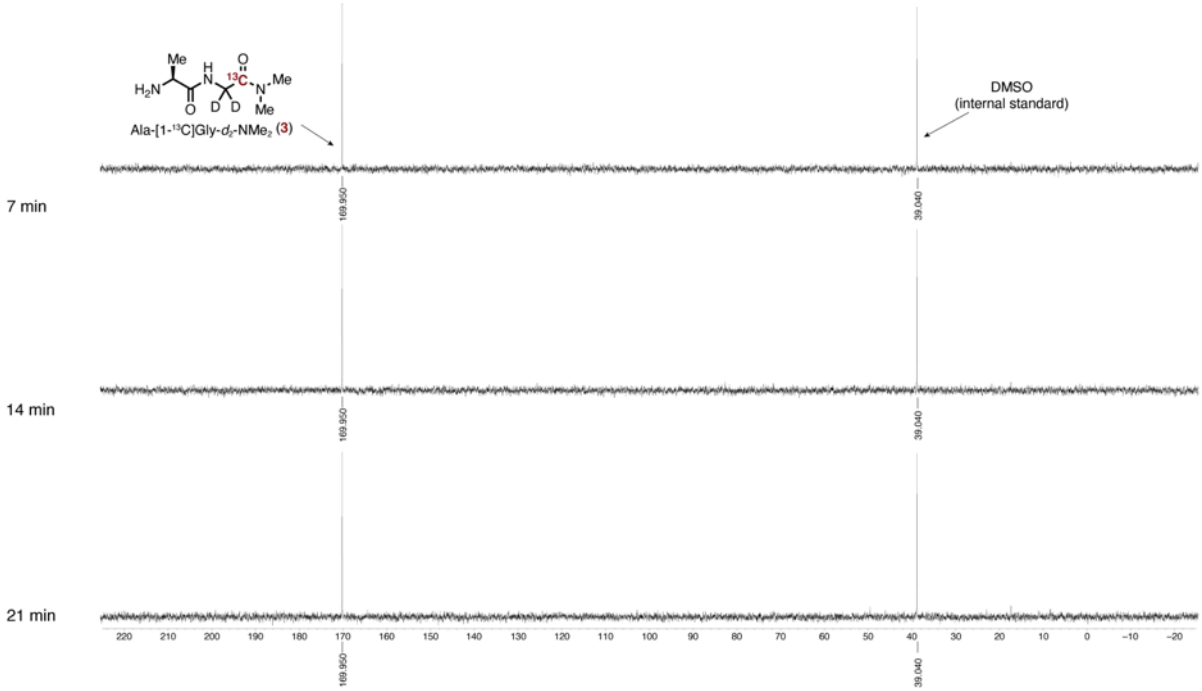

Fig. S8. Thermally equilibrated ^{13}C NMR spectra of Ala-[1-^{13}C]Gly-d_2-NMe_2 incubated in homogenate of mouse tumor xenograft (MIA PaCa-2), in the presence of phebestin as an APN-inhibitor.

Stability of Ala-[1-^{13}C]Gly-d_2-NMe$_2$ in mouse serum

We assessed the stability of Ala-[1-^{13}C]Gly-d_2-NMe$_2$ (**3**) in mouse serum. There is a concern that Ala-[1-^{13}C]Gly-d_2-NMe$_2$ may be metabolized in blood before reaching at the region of interest because APN is known to also exist in blood as a soluble form (43). In this experiment, no conversion of Ala-[1-^{13}C]Gly-d_2-NMe$_2$ was observed within 21 min after incubation in mouse serum. After 28 min incubation, the peak of the metabolite [1-^{13}C]Gly-d_2 (**4**) was gradually appeared. The detailed procedure is described in Materials and Methods section.

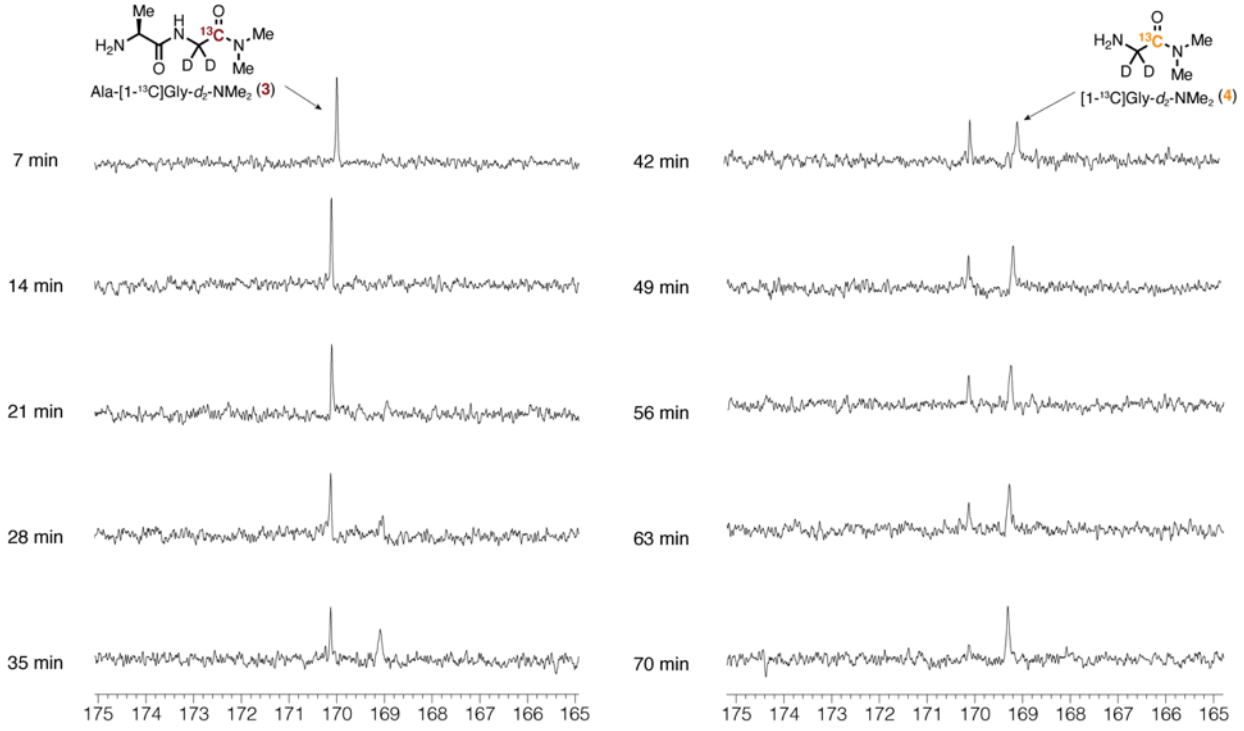

Fig. S9. Thermally equilibrated ^{13}C NMR spectra of Ala-[1-^{13}C]Gly-d_2-NMe$_2$ incubated in mouse serum.

Measurement conditions, 10 mM Ala-[1-^{13}C]Gly-d_2-NMe$_2$ (**3**), mouse serum containing 10% D_2O, 37 °C (flip angle: 30°, relaxation delay: 2 s, 128 scans (*ca.* 7 min)).

5. *In vivo* experiment under hyperpolarized state

Recovery experiment in the hyperpolarized study for *in vivo* detection of APN activity

In the study for detection of APN-activity *in vivo* shown in Fig. 6, we confirmed the recovery of APN-activity one day after administration of phebestin (fig. S10). This result indicates that the DNP-MRS with the current APN probe enables repetitive measurements without affecting APN-activity.

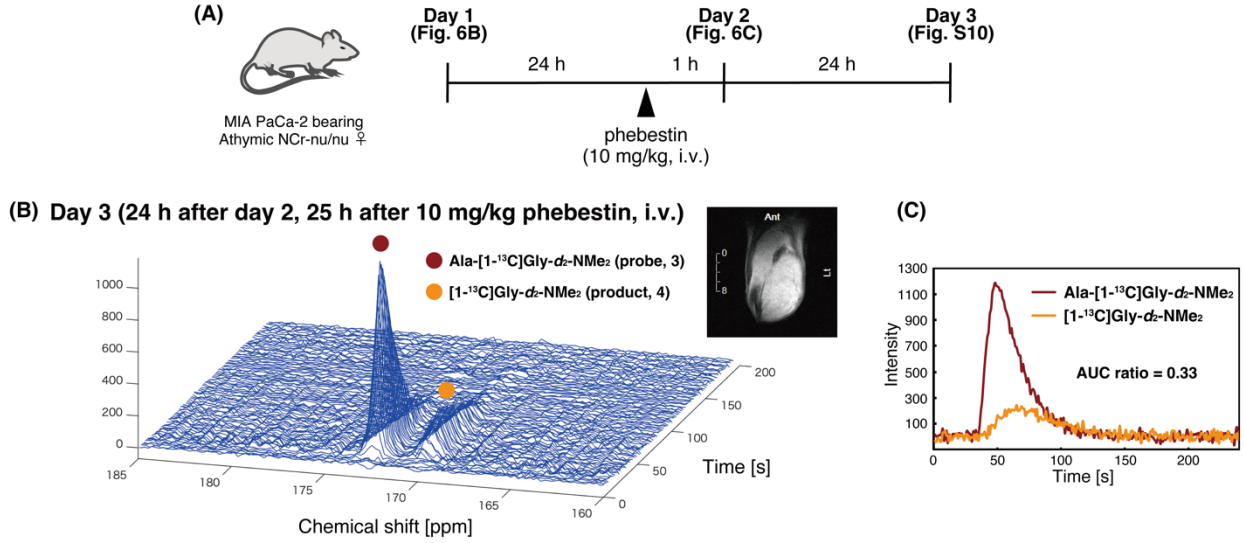

Fig. S10. Recovery experiment in the hyperpolarized study for *in vivo* detection of APN activity in human pancreatic tumor xenograft bearing mouse.

(**A**) Schematic representation of the experimental outlines. (**B**) Time series of ^{13}C NMR spectra acquired *in vivo* with the coil placed over the leg tumor, after the intravenous injection of hyperpolarized probe **3**. Inset figure: an example of the anatomical image from the observed area (^{1}H MRI). (**C**) Time-course plots of ^{13}C signals of Ala-[1-^{13}C]Gly-d_2-NMe$_2$ (**3**) (red line) and [1-^{13}C]Gly-d_2-NMe$_2$ (**4**) (orange line). AUC, area under the curve.

Chemical shift imaging of APN activity

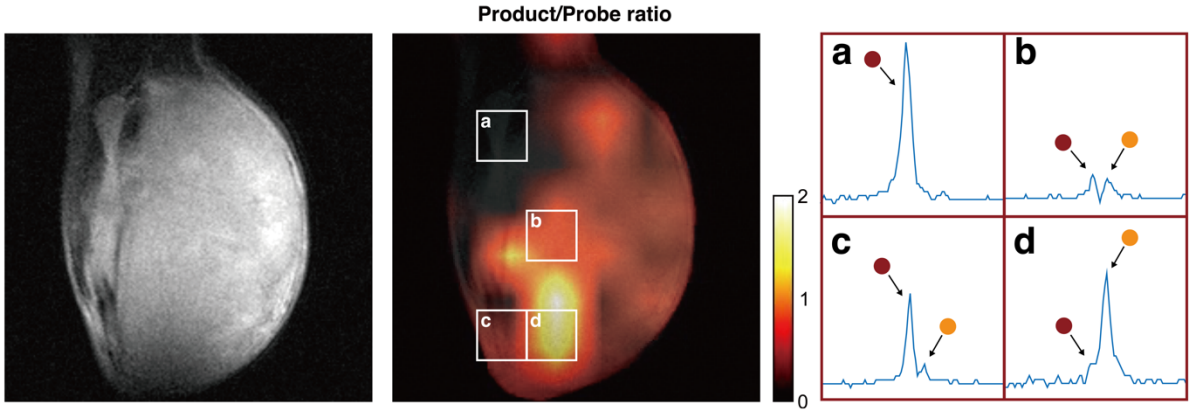

Fig. S11. Additional experimental data of chemical shift imaging of a mouse leg bearing xenograft tumor (MIA PaCa-2).

Chemical shift imaging of a mouse leg bearing xenograft tumor (MIA PaCa-2). (left) Anatomical image from the observed area (T_2-weighted ^{1}H MRI). (middle) Image of the product (**4**) to the probe (**3**) ratio. (right) Expanded spectra in representative voxels a–d. The voxel size is 2.8 mm × 2.8 mm × 10 mm. The left peak is Ala-[1-^{13}C]Gly-d_2-NMe$_2$ (**3**, red circle), and the right peak is [1-^{13}C]Gly-d_2-NMe$_2$ (**4**, orange circle). The image was acquired at 18 s to 26 s after injection of the hyperpolarized probe. ^{13}C spectra are with denoising process.

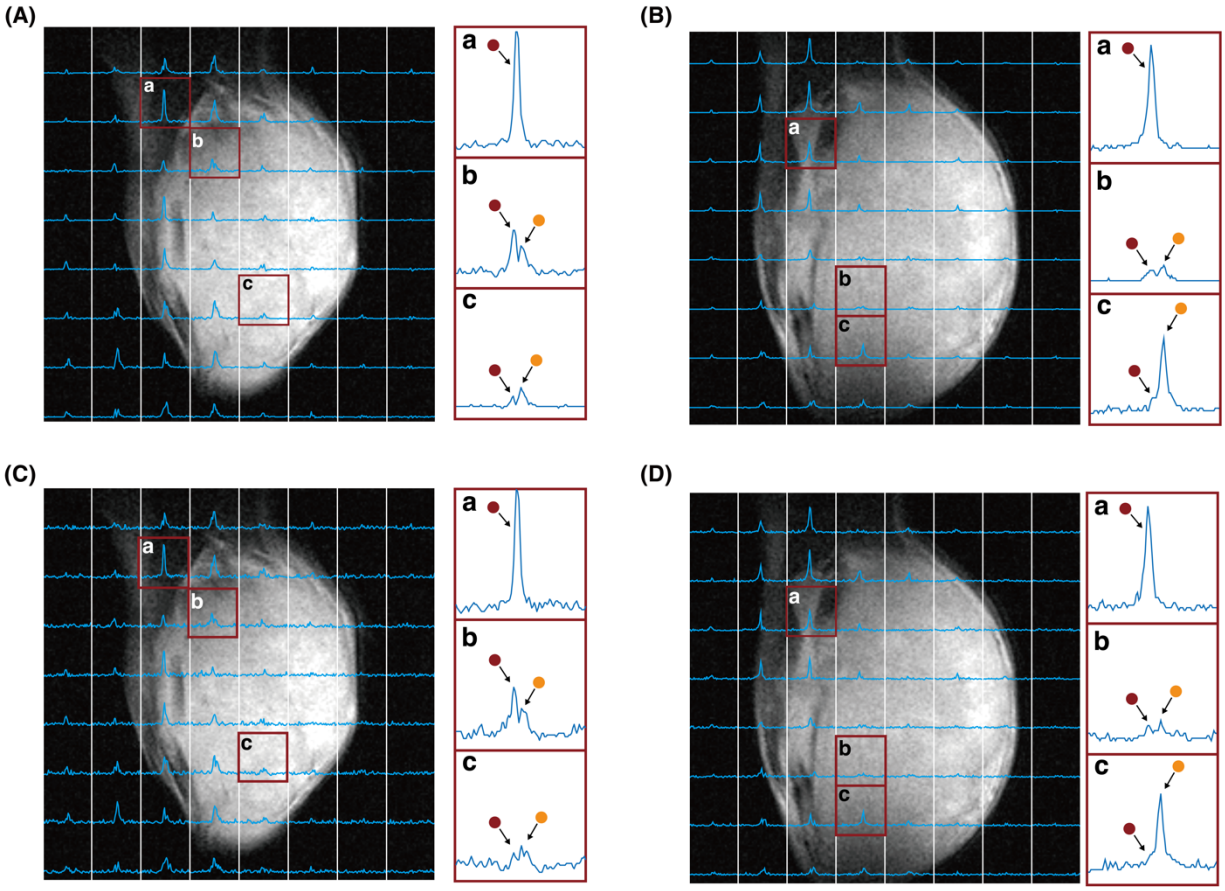

Fig. S12. Chemical shift imaging of mouse legs bearing xenograft tumors (MIA PaCa-2) with (A and B) or without (C and D) denoising process.

The voxel size is 2.8 mm × 2.8 mm × 10 mm. Inset figure: expanded spectra in representative voxels a–c. The left peak is Ala-[1-^{13}C]Gly-d_2-NMe$_2$ (**3**, red circle), and the right peak is [1-^{13}C]Gly-d_2-NMe$_2$ (**4**, orange circle). figs. S12A and S12C correspond to Fig. 6G; figs S12B and S12D correspond to fig. S11, respectively. ^{13}C spectra of figs. S12A and S12B are with denoising process; ^{13}C spectra of figs. S12C and S12D are without denoising process.

6. Magnetic field dependency and R_1^{CSA}

T_1 and R_1 of Ala-[1-^{13}C]Gly-d_2-NMe$_2$ were measured at 9.4, 11.7, and 14.1 T. The results are summarized in fig. S13. R_1 values were proportional to the square of the magnetic field (B_0^2). This trend indicates that R_1^{CSA} is much larger than the other B_0-dependent R_1 factors. From this plot, the R_1^{CSA} of Ala-[1-^{13}C]Gly-d_2-NMe$_2$ can be determined as the product of the coefficient of the approximate line and the square of magnetic field strength (44, 45). The R_1^{CSA} at 9.4 T was 14.9 × 10^{-3} s^{-1}. The T_1 at 3.0 T was predicted to be 62.5 s.

B_0 (T)	B_0^2 (T^2)	T_1 (s)	R_1 (×10^{-3} s^{-1})
9.4	88.4	34.2 ± 3.0	29.4 ± 2.6
11.7	136.9	26.7 ± 1.0	37.5 ± 1.5
14.1	198.8	20.8 ± 0.7	48.0 ± 1.7

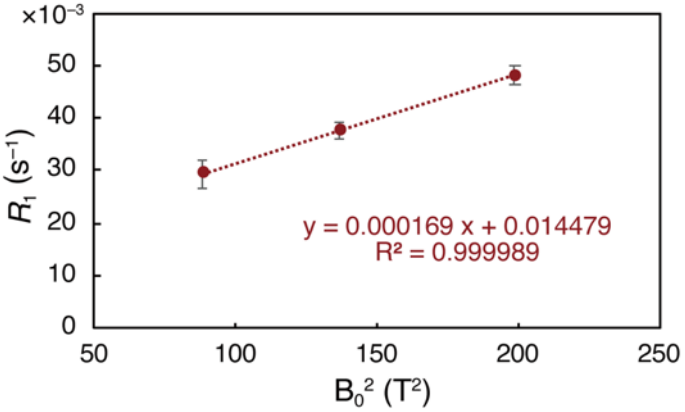

Fig. S13. Magnetic field dependency of R_1 of Ala-[1-^{13}C]Gly-d_2-NMe$_2$.
Measurement conditions, 10 mM Ala-[1-^{13}C]Gly-d_2-NMe$_2$ in D_2O, 37 °C, inversion recovery method. (n = 3).

7. T_1 values of candidate compounds at 3.0 T under hyperpolarized state

Table S1. T_1 values measured at 3.0 T under hyperpolarized state[a]

Compound	Conditions					
	DPBS, 37 °C	Serum (67%), 37 °C	DPBS, r.t.	Serum (86%), 37 °C	D_2O, 37 °C	PB, 37 °C
Ala-[1-^{13}C]Gly-d_2-NMe_2 (**3**)	56.7 ± 8.7 s	43.4 s	43.7 ± 1.1 s	44.6 s	63.8 s	58.3 s
[1-^{13}C]Ala-NH_2 (**5**)	35.7 s	33.4 s				
[1-^{13}C]Ala-NHMe (**6**)	36.5 s	32.2 s				
[1-^{13}C]Ala-Gly (**7**)	29.3 s	24.7 s				
[1-^{13}C]Ala-Ala (**8**)	21.7 s	17.8 s				
[1-^{13}C]Ala-D-Ala (**9**)	22.7 s	18.6 s				
[1-^{13}C]Ala-β-Ala (**10**)	22.4 s	21.8 s				
[1-^{13}C]Ala-Gly-NMe_2 (**11a**)	22.8 s	20.1 s				
Ala-[1-^{13}C]Gly-NMe_2 (**11b**)	30.1 s	28.1 s				

[a]The corrected T_1 values are shown. The corrected T_1 values were calculated from apparent T_1 values considering the magnetization loss due to successive flip angles. Dissolved hyperpolarized solution (DPBS containing 0.68 mM EDTA, 1.0 mL) was added into 2.0 mL of DPBS, human serum, D_2O or phosphate buffer (PB, 100 mM, pH = 7.4), and then subjected to T_1 measurement (3.0 T, *ca*. 37 °C).

8. Materials and Methods

8-1. General

Synthesis

Unless otherwise noted, all materials including dry solvents were obtained from commercial suppliers and used without further purification. Unless otherwise noted, work-up and purification procedures were performed with reagent-grade solvents under air. Analytical thin-layer chromatography (TLC) was performed using E. Merk silica gel 60 F_{254} precoated plates (0.25 mm). The developed chromatogram was analyzed with UV lamp (254 nm) and ethanolic ninhydrin. Flash column chromatography was performed with silica gel 60N (Kanto Chemical Co., spherical, neutral, 40–50 μm) in manual operation, or with an Isolera Spektra instrument equipped with a Biotage® Sfär Silica HC D 10 g or Sfär Silica HC D 25 g cartridge in automatic operation.

Compounds

Ala-NH_2·HCl, Ala-NHMe·HCl, Ala-Gly, and Ala-Ala were purchased from Fujifilm Wako Pure Chemical (Osaka, Japan), BACHEM (Bubendorf, Switzerland), Sigma-Aldrich (St. Louis, USA), Sigma-Aldrich (St. Louis, USA), respectively. Ala-Gly-NMe_2 and Ala-Gly-NHMe were synthesized with referring to the protocol of Ala-[1-^{13}C]Gly-d_2-NMe_2 (shown below) without the deuteration step.

How to treat the current probe (Ala-[1-^{13}C]Gly-d_2-NMe_2)

Because Ala-[1-^{13}C]Gly-d_2-NMe_2 is air-sensitive as a free-amine form, this compound should be treated quickly under air and stored in inert gas. After neutralization in aqueous solution, this compound is relatively stable but long storage in acidic condition causes decomposition. This compound is highly hygroscopic, and does not become solid easily, so that lyophilization may be needed to be repeated a few times. Although the solution turned brown or red sometimes during lyophilization (probably, due to oxidation), the samples could be used for hyperpolarization without any problems.

Measurements

High-resolution mass spectrometry (HRMS) was measured using a Bruker micrOTOF II (ESI). Nuclear magnetic resonance (NMR) spectra were recorded on a JEOL ECS400 (^{1}H 400 MHz, ^{13}C 100 MHz) spectrometer. Chemical shifts for ^{1}H NMR are expressed in parts per million (ppm) relative to tetramethylsilane (δ 0.00 ppm) in $CDCl_3$, HOD (δ 4.79 ppm) in D_2O. Chemical shifts for ^{13}C NMR are expressed in ppm relative to $CDCl_3$ (δ 77.2 ppm) in $CDCl_3$, 1,4-dioxane (δ 67.2 ppm) or MeOH (δ 49.5 ppm) in D_2O for synthesis, and DMSO (δ 39.04 ppm) for evaluation experiment. Data are reported as follows: chemical shift, multiplicity (s = singlet, brs = broad singlet, d = doublet, t = triplet, q = quartet, qui = quintet, sep = septet, m = multiplet), coupling constant (Hz), and integration. HPLC analyses were performed using a COSMOSIL® 5C18-MS-II (4.6 mm × 150 mm) column (Nacalai tesque) on an HPLC system composed of a pump (LC-20AT, Shimadzu) and a detector (RF-10A, Shimadzu).

Hyperpolarized studies were performed by a Hypersense DNP polarizer (Oxford Instruments, UK) using microwave irradiation at 94.069 GHz and 100 mW under 2.8 mbar at 1.45 K, and a 3

T MR Solutions animal scanner (MR SOLUTIONS Ltd., USA). The signal processing of MRS data was performed using the low rank denoising technique as described previously (41).

Abbreviation
Boc: *tert*-butoxycarbonyl
Cbz: benzyloxycarbonyl
DCC: *N*,*N′*-dicyclohexylcarbodiimide
DMF: *N*,*N*-dimethylformamide
DMSO: dimethyl sulfoxide
DPBS: Dulbecco's phosphate buffer saline
EDCI: 1-ethyl-3-(3-dimethylaminopropyl)carbodiimide
EDTA: ethylenediaminetetraacetic acid
HOBt: 1-hydroxybenzotriazole
NBD-F: 4-fluoro-7-nitrobenzofurazan
Su: succinylimidyl
TFA: trifluoroacetic acid

8-2. Binding energy calculations

The substrate-APN structures for Ala-NH_2-APN, Ala-Gly-APN, and Ala-Gly-NMe_2-APN were modeled, using the E384Q mutant crystal structure with polyalanine (PDB ID: 4NAQ) and replacing the Gln384 side chain with glutamate (32). Hydrogen atoms and the Glu384 side-chain were energetically optimized with CHARMM version 40b (46), while the positions of all non-hydrogen atoms were fixed, and all titratable atoms groups were maintained in their standard protonation states at pH 7 (i.e., acidic groups were ionized, and basic groups were protonated) if not otherwise specified. The protonation pattern of the titratable residues was calculated, solving the linear Poisson-Boltzmann equation with the MEAD program (47). The difference in electrostatic energy between the two protonation states, protonated and deprotonated, in a reference model system was calculated using a known experimentally measured pK_a value (e.g., 4.0 for Asp (48)). The difference in the pK_a value of the protein relative to the reference system was added to the known reference pK_a value. The experimentally measured pK_a values employed as references were 12.0 for Arg, 4.0 for Asp, 9.5 for Cys, 4.4 for Glu, 10.4 for Lys, 9.6 for Tyr (48), and 7.0 and 6.6 for the N_ε and N_δ atoms of His, respectively (49–51). All other titratable sites were fully equilibrated to the protonation state of the target site during titration. The dielectric constants were set to 4 for the protein interior and 80 for water. All other water molecules, whose hydrogen bond orientations were not specifically reported, were considered implicitly. All computations were performed at 300 K, pH 7.0, and with an ionic strength of 100 mM. The linear Poisson-Boltzmann equation was solved using a three-step grid-focusing procedure at resolutions of 2.5, 1.0, and 0.3 Å. The ensemble of the protonation patterns was sampled by the Monte Carlo (MC) method with the Karlsberg program (52). The MC sampling yielded the probabilities [protonated] and [deprotonated] of the two protonation states of the molecule. Using the calculated protonation pattern, hydrogen atoms of the protonated residues were generated explicitly. The geometry was optimized using a QM/MM approach. The restricted density functional theory (DFT) method was employed with the B3LYP functional and LACVP* basis sets using the QSite program (53). The QM region was defined as substrate, Zn^{2+}, water molecules (HOH-104, 1218,

and 1776), the side chains of Gln208, Glu350, Glu384, His383, His387, Glu406, and Tyr472, and the side chain and backbone of Ala348. All atomic coordinates were fully relaxed in the QM region. In the MM region, the positions of hydrogen atoms were optimized using the OPLS2005 force field (54), while the positions of the heavy atoms were fixed. The binding energy between the substrate and APN was calculated based on the QM/MM-optimized structure, using the MOE program (55). See Data S1 for the QM/MM-optimized atomic coordinates.

8-3. Synthesis

Synthesis of **S2** (36)

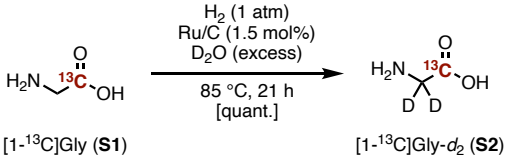

To a 50-mL round-bottom flask containing a magnetic stirring bar were added [1-^{13}C]Gly (**S1**) (304 mg, 4.00 mmol), ruthenium on activated carbon (121 mg, 1.5 mol% for Ru, 5%wt), and D_2O (7.0 mL). The vessel was equipped with a condenser and a H_2 balloon. After evacuation of air and filling back H_2 (repeated three times), the mixture was stirred at 85 °C for 21 h. After cooling to room temperature, the resulting mixture was filtrated through Celite®. The filtrate was concentrated under reduced pressure. The deuterated product (**S2**) was obtained (313 mg, quant.) as a yellowish solid. This product was used for the next step without further purification and characterization.

Synthesis of **S3**

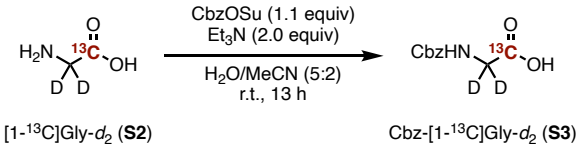

To a 25-mL round-bottom flask containing a magnetic stirring bar were added [1-^{13}C]Gly-d_2 (**S2**) (313 mg, 4.00 mmol) and H_2O (3.0 mL). After addition of Et_3N (1.12 mL, 2.0 equiv), *N*-(benzyloxycarbonyloxy)succinimide (CbzOSu, 1.05 g, 1.1 equiv) in MeCN (1.2 mL) was added into the vessel. The mixture was stirred at room temperature for 13 h. The resulting mixture was evaporated to remove MeCN and Et_3N. To the remained aqueous solution was added saturated $NaHCO_3$ aq. (10 mL), and then the solution was washed with Et_2O (5.0 mL). The aqueous phase was acidified with 1 M HCl aq. to adjust pH into *ca.* 3. When white precipitation appeared, the resulting mixture was extracted with EtOAc (15 mL × 6). The organic phase was dried over anhydrous Na_2SO_4, filtrated, and concentrated under reduced pressure. The residue was confirmed to contain the desired product **S3** and hydroxysuccinimide with ^{1}H NMR. This crude was used for the next step without further purification.

Synthesis of **S4**

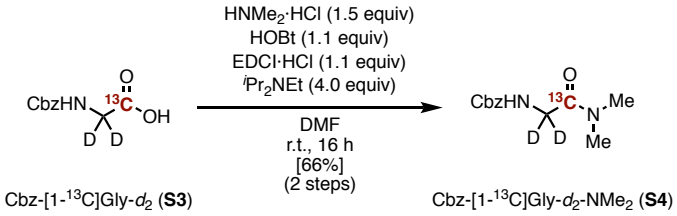

To a 100-mL round-bottom flask containing a magnetic stirring bar was added the crude of the above reaction theoretically containing 4.00 mmol of Cbz-[1-^{13}C]Gly-d_2 (**S3**). Dimethylamine hydrochloride (487 mg, 1.5 equiv), HOBt (595 mg, 1.1 equiv), and EDCI·HCl (843 mg, 1.1 equiv) were added to the vessel, successively. After purging N_2 by evacuation and filling back N_2 three times, DMF (13 mL) and diisopropylethylamine (2.79 mL, 4.0 equiv) were added. The mixture was stirred for 16 h at room temperature, and then evaporated to remove solvents. The residue was dissolved into CH_2Cl_2 and added H_2O. The two-phase solution was extracted with CH_2Cl_2 (10 mL × 2). The organic phase was washed with saturated Na_2CO_3 aq. (20 mL × 2) and brine (7.0 mL × 1), dried over anhydrous Na_2SO_4, filtrated, and concentrated under reduced pressure. The residue was subjected to silica-gel column chromatography (CH_2Cl_2/MeOH = 20:0 to 19:1) to afford Cbz-[1-^{13}C]Gly-d_2-NMe_2 (**S4**) (636 mg, 66% yield through two steps from **S2**) as a yellowish clear oil.

S4: ^{1}H NMR (400 MHz, $CDCl_3$) δ 7.40–7.29 (m, 5H), 5.78 (brs, 1H), 5.13 (s, 2H), 3.99 (brs, 0.18H, deuterated position), 2.98 (d, J = 2.4 Hz, 3H), 2.97 (d, J = 3.2 Hz, 3H); ^{13}C NMR (100 MHz, $CDCl_3$) δ 168.0 (labeled), 156.4, 136.6, 128.6, 128.2, 128.1, 66.9, 42.5 (brs, deuterated carbon), 35.9, 35.7; HRMS (ESI) *m/z* calcd for $C_{11}{}^{13}CH_{14}D_2N_2NaO_3$ $[M+Na]^+$: 262.1212, found 262.1212.

Synthesis of **4**

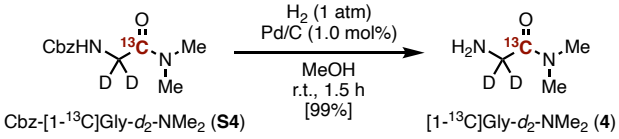

To a 50-mL round-bottom flask containing a magnetic stirring bar were added Cbz-[1-^{13}C]Gly-d_2-NMe_2 (**S4**) (636 mg, 2.66 mmol) and palladium on activated carbon (28.3 mg, 1.0 mol% for Pd, 10%wt). The vessel was equipped with a three-way cock and a N_2 balloon, and then purged with N_2 through evacuation and filling back N_2 three times. After addition of MeOH (13 mL), the N_2 balloon was replaced with a H_2 balloon, and the vessel was purged with H_2. The mixture was stirred for 1.5 h and filtered through Celite®. The filtrate was concentrated under reduced pressure. The desired compound [1-^{13}C]Gly-d_2-NMe_2 (**4**) was obtained (276 mg, 99% yield) as a colorless oil.

4: ^{1}H NMR (400 MHz, $CDCl_3$) δ 2.98 (d, J = 2.4 Hz, 3H), 2.94 (d, J = 2.8 Hz, 3H), 1.66 (brs, 2H); ^{13}C NMR (100 MHz, $CDCl_3$) δ 172.7 (labeled), 42.9 (brs, deuterated carbon), 35.8, 35.7; HRMS (ESI) *m/z* calcd for $C_3{}^{13}CH_8D_2N_2NaO$ $[M+Na]^+$: 128.0844, found 128.0846.

Synthesis of **S5**

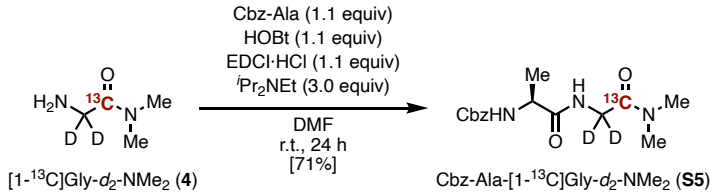

To a 50-mL round-bottom flask containing a magnetic stirring bar were added [1-^{13}C]Gly-d_2-NMe_2 (**4**) (276 mg, 2.63 mmol), Cbz-Ala (645 mg, 2.89 mmol, 1.1 equiv), HOBt (391 mg, 2.89 mmol, 1.1 equiv), and EDCI·HCl (555 mg, 2.89 mmol, 1.1 equiv), successively. The vessel was equipped with a three-way cock and a N_2 balloon, and then purged with N_2 through evacuation and filling back N_2 three times. After addition of DMF (13 mL) and ^{i}Pr$_2$NEt (1.37 mL, 7.86 mmol, 3.0 equiv), the mixture was stirred for 24 h. The resulting solution was evaporated to reduce solvents. The residue was added CH_2Cl_2 and H_2O, and extracted with CH_2Cl_2 (12 mL × 3). The organic phase was washed with saturated $NaHCO_3$ aq. (5 mL × 2), dried over anhydrous Na_2SO_4, filtrated, and concentrated under reduced pressure. The residue was subjected to silica-gel column chromatography (CH_2Cl_2/MeOH = 20:0 to 19:1) then (EtOAc/MeOH = 10:0 to 9:1) to afford Cbz-Ala-[1-^{13}C]Gly-d_2-NMe_2 (**S5**) (580 mg, 71% yield) as a white solid.

S5: ^{1}H NMR (400 MHz, $CDCl_3$) δ 7.41–7.30 (m, 5H), 6.92 (brs, 1H), 5.34 (brs, 1H), 5.16–5.07 (m, 2H), 4.33–4.30 (m, 1H), 4.02 (brs, 0.18H, deuterated position), 3.00 (d, J = 2.4 Hz, 3H), 2.98 (d, J = 3.2 Hz, 3H), 1.41 (d, J = 7.2 Hz, 3H); ^{13}C NMR (100 MHz, $CDCl_3$) δ 172.5, 167.8 (labeled), 156.0, 136.5, 128.7, 128.3, 67.1, 50.7, 36.1, 35.7, 19.3, One carbon was not observed due to overlapping. One carbon (deuterated) was not observed due to broadening.; HRMS (ESI) *m/z* calcd for $C_{14}{}^{13}CH_{19}D_2N_3NaO_4$ $[M+Na]^+$: 333.1583, found 333.1585.

Synthesis of **3**

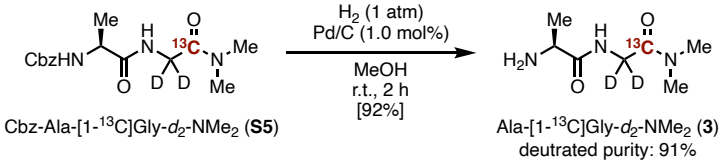

To a 2-necked 30-mL round-bottom flask containing a magnetic stirring bar were added Cbz-Ala-[1-^{13}C]Gly-d_2-NMe_2 (**S5**) (310 mg, 1.00 mmol) and palladium on activated carbon (10.5 mg, 1.0 mol% for Pd, 10%wt). The vessel was equipped with a three-way cock and a N_2 balloon, and then purged with N_2 through evacuation and filling back N_2 three times. After addition of MeOH (5.0 mL), the N_2 balloon was replaced with a H_2 balloon, and the vessel was purged with H_2. The mixture was stirred for 2 h and filtered through Celite®. The filtrate was concentrated under reduced pressure. The desired compound Ala-[1-^{13}C]Gly-d_2-NMe_2 (**3**) was obtained (162 mg, 92% yield) as a colorless oil. The deuterated purity at α-position of Gly-moiety was calculated as 91% with ^{1}H NMR.

3: ^{1}H NMR (400 MHz, $CDCl_3$) δ 7.91 (brs, 1H), 4.04–4.02 (m, 0.18H, deuterated position), 3.56–3.48 (m, 1H), 3.00 (s, 3H), 3.00 (s, 3H), 1.46 (brs, 2H), 1.35 (d, J = 6.8 Hz, 3H); ^{13}C NMR

(100 MHz, $CDCl_3$) δ 176.1, 168.1 (labeled), 50.8, 41.2–39.6 (m, deuterated carbon), 36.0, 35.5, 21.7; HRMS (ESI) *m/z* calcd for $C_6{}^{13}CH_{13}D_2N_3NaO_2$ $[M+Na]^+$: 199.1216, found 199.1228.

Synthesis of **S6** for Ala-D-Ala (**9**)

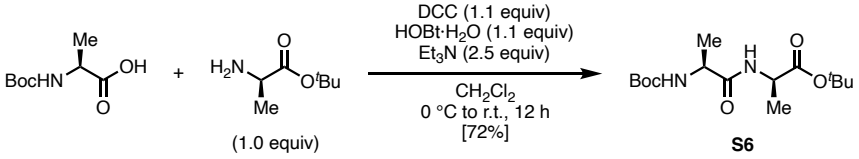

To a 2-necked 50-mL round-bottom flask containing a magnetic stirring bar were added Boc-Ala (190 mg, 1.00 mmol), D-Ala-O^{t}Bu (146 mg, 1.00 mmol, 1.0 equiv), DCC (231 mg, 1.12 mmol, 1.1 equiv), and HOBt·H_2O (169 mg, 1.10 mmol, 1.1 equiv), successively. The vessel was equipped with a three-way cock and a N_2 balloon, and then purged with N_2 through evacuation and filling back N_2 three times. The vessel was cooled in an ice bath. After addition of DMF (10 mL) and Et_3N (348 μL, 2.50 mmol, 2.5 equiv), the ice bath was removed, and the mixture was stirred at room temperature for 12 h. The resulting solution was added CH_2Cl_2 (20 mL) and washed with 0.1 M HCl aq. (10 mL), saturated $NaHCO_3$ aq. (10 mL), and brine. The organic phase was dried over anhydrous Na_2SO_4, filtrated, and concentrated under reduced pressure. The residue was subjected to silica-gel column chromatography (hexane/EtOAc = 5:1 then hexane/EtOAc = 2:1) to afford Boc-Ala-D-Ala-O^{t}Bu (**S6**) (235 mg, 74% yield) as a white solid.

S6: ^{1}H NMR (400 MHz, $CDCl_3$) δ 6.62–6.61 (m, 1H), 4.96 (brs, 1H), 4.44 (qui, J = 6.8 Hz, 1H), 4.19 (brs, 1H), 1.47 (s, 9H), 1.45 (s, 9H), 1.37 (d, J = 6.8 Hz, 3H), 1.36 (d, J = 6.8 Hz, 3H); ^{13}C NMR (100 MHz, $CDCl_3$) δ 172.2, 172.1, 155.6, 82.2, 80.4, 50.4, 48.8, 28.5, 28.1, 18.7, 18.6; HRMS (ESI) *m/z* calcd for $C_{15}H_{28}N_2NaO_5$ $[M+Na]^+$:339.1890, found 339.1891.

Synthesis of Ala-D-Ala·HCl (**9**·HCl)

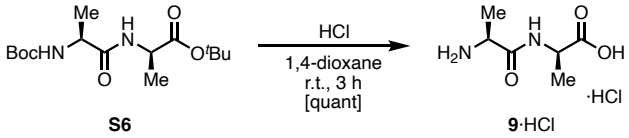

To a 25-mL round-bottom flask containing a magnetic stirring bar was added Boc-Ala-D-Ala-O^{t}Bu (**S6**) (148 mg, 467 μmol). After 4 N HCl in 1,4-dioxane (2.0 mL) was added, the mixture was stirred at room temperature for 3 h. The resulting solution was concentrated under reduced pressure. The desired compound Ala-D-Ala·HCl (**9**·HCl) was obtained (121 mg, quant.) as a white powder.

9: ^{1}H NMR (400 MHz, D_2O) δ 4.40 (q, J = 7.2 Hz, 1H), 4.12 (q, J = 7.2 Hz, 1H), 1.55 (d, J = 6.8 Hz, 3H), 1.46 (d, J = 7.2 Hz, 3H); ^{13}C NMR (100 MHz, D_2O) δ 177.0, 171.2, 49.6, 49.5, 17.1, 16.7; HRMS (ESI) *m/z* calcd for $C_6H_{12}N_2NaO_3$ $[M+Na]^+$: 183.0740, found 183.0740.

Synthesis of **S7** for Ala-β-Ala (**10**)

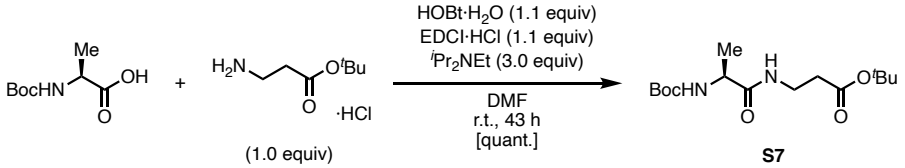

To a 2-necked 50-mL round-bottom flask containing a magnetic stirring bar were added Boc-Ala (567 mg, 3.00 mmol), β-Ala-O^{t}Bu·HCl (547 mg, 3.01 mmol, 1.0 equiv), HOBt·H_2O (506 mg, 3.30 mmol, 1.1 equiv), and EDCI·HCl (634 mg, 3.31 mmol, 1.1 equiv), successively. The vessel was equipped with a three-way cock and a N_2 balloon, and then purged with N_2 through evacuation and filling back N_2 three times. After addition of DMF (15 mL) and ^{i}Pr$_2$NEt (1.57 mL, 9.01 mmol, 3.0 equiv), the mixture was stirred for 43 h. The resulting solution was evaporated to reduce solvents. The residue was added H_2O and extracted with EtOAc (20 mL × 2). The organic phase was washed with brine, dried over anhydrous Na_2SO_4, filtrated, and concentrated under reduced pressure. The residue was subjected to silica-gel column chromatography (hexane/EtOAc = 1:1 and hexane/EtOAc = 2:1) to afford Boc-Ala-β-Ala-O^{t}Bu (**S7**) (948 mg, quant.) as a colorless oil.

S7: ^{1}H NMR (400 MHz, $CDCl_3$) δ 6.60 (brs, 1H), 5.02 (brs, 1H), 4.12 (brs, 1H), 3.55–3.43 (m, 2H), 2.44 (t, J = 6.0 Hz, 2H), 1.45 (s, 9H), 1.44 (s, 9H), 1.34 (d, J = 7.2 Hz, 3H); ^{13}C NMR (100 MHz, $CDCl_3$) δ 172.8, 171.7, 155.5, 81.2, 80.0, 77.4, 50.2, 35.2, 28.4, 28.2, 18.8; HRMS (ESI) *m/z* calcd for $C_{15}H_{28}N_2NaO_5$ $[M+Na]^+$: 339.1890, found 339.1890.

Synthesis of Ala-β-Ala·HCl (**10**·HCl)

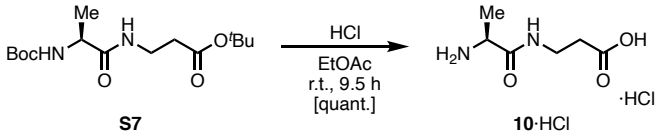

To a 30-mL round-bottom flask containing a magnetic stirring bar was added Boc-Ala-β-Ala-O^{t}Bu (**S7**) (640 mg, 2.02 mmol). After 4 N HCl in EtOAc (2.0 mL) was added, the mixture was stirred at room temperature for 9.5 h. During this reaction, further 4 N HCl in EtOAc (1.0 mL) was added after 7 h. MeOH and H_2O were added to the vessel and the resulting solution was concentrated under reduced pressure. The desired compound Ala-β-Ala·HCl (**10**·HCl) was obtained (256 mg, quant.).

10: ^{1}H NMR (400 MHz, D_2O) δ 4.07–4.01 (m, 1H), 3.62–3.44 (m, 2H), 2.67–2.63 (m, 2H), 1.51 (d, J = 7.2 Hz, 3H), Small peaks of the cis-form were observed at 1.50 (d, J = 7.6 Hz); ^{13}C NMR (100 MHz, D_2O) δ 172.9, 167.7, 46.2, 32.3, 30.4, 13.7, Small peaks of the cis-form were observed at 171.6, 46.0, 32.4, 30.5.; HRMS (ESI) *m/z* calcd for $C_6H_{12}N_2NaO_3$ $[M+Na]^+$: 183.0740, found 183.0740.

8-4. Biochemical experiments

Expression and purification of recombinant human APN

The cDNA coding human aminopeptidase N (D66-K967, Uniprot ID: P15144) was cloned by PCR from cDNA library of A204 cells (primers are shown below) and subcloned into the expression vector pEFs (42). The leader sequence of the immunoglobulin kappa chain and hexa-histidine tag were fused at the N-terminus and C-terminus, respectively. A proline residue was inserted between the leader sequence and APN-coding sequence. The expression and purification of the proteins were conducted as previously described (56). Expi293F cells were transfected with the expression vector and cultured according to the manufacturer's protocol. After 4 days of culture, the cells were centrifuged at 3000 × *g* for 30 min at 4 °C, and the supernatant was dialyzed at 4 °C against nickel-nitrilotriacetic acid (Ni-NTA)-binding buffer (20 mM Tris-HCl (pH = 7.6 at r.t.), 500 mM NaCl, and 5 mM imidazole). The dialyzed samples were purified using Ni-NTA agarose beads (#30210, QIAGEN) and Econo-Pac Chromatography Columns (Bio-Rad). The eluted samples were dialyzed against size exclusion chromatography (SEC) buffer (10 mM HEPES (pH = 7.4 at r.t.), and 50 mM NaCl) and purified using a Superdex 26/60 column (GE Healthcare). The concentration of the protein was determined by measuring the absorbance at 280 nm using a NanoDrop ND-1000 (Thermo Fisher Scientific). The purity of the final preparation was checked by sodium dodecyl sulfate-polyacrylamide gel electrophoresis (SDS-PAGE) and Coomassie Brilliant Blue (CBB) staining.

Primers for cloning of cDNA coding hAPN
Fw: 5′-GACCAAAGTAAAGCGTGGAATCGTTACC-3′
Rv: 5′-TTTGCTGTTTTCTGTGAACCACTGGAG-3′

Enzymatic reaction for exploration of probe candidates (Fig. 3A)

The solution of the compound (6.0 mM) in phosphate buffer (50.0 μL, 100 mM, pH = 7.4) was preincubated at 37 °C for 10 min. To the vessel was added the solution of 19.4 nM recombinant human APN in phosphate buffer (50.0 μL, 100 mM, pH = 7.4) preincubated at 37 °C for 10 min. The resulting solution (100 μL, 3.0 mM the compound, 9.7 nM human APN) was incubated at 37 °C for 40 min. The reaction was quenched by addition of an inhibitor solution (20.0 μL, 25 mM EDTA, 5.0 mM 1,10-phenanthroline in H_2O). After mixing, the solution was immediately cooled on ice. 100 μL of the solution was added to 400 μL of D_2O containing 1,4-dioxane (an internal standard for chemical shift). The conversion of the compound was determined with ^1H NMR.

Time-dependent enzymatic reaction of Ala-NH_2 and Ala-Gly-NMe_2 (Fig. 3C)

The solution of the compound (6.0 mM) in phosphate buffer (130 μL, 100 mM, pH = 7.4) was preincubated at 37 °C for 10 min. To the vessel was added the solution of 19.4 nM human APN in phosphate buffer (130 μL, 100 mM, pH = 7.4) preincubated at 37 °C for 10 min. The resulting solution (260 μL, 3.0 mM the compound, 9.7 nM recombinant human APN) was incubated at 37 °C and 50.0 μL was sampled every 5 minutes for 5–25 min. The sampled solution was added immediately to an inhibitor solution (10.0 μL, 25 mM EDTA, 5.0 mM 1,10-phenanthroline in H_2O) for quenching the reaction. After mixing, the solution was added to 450 μL of D_2O containing 1,4-dioxane (an internal standard for chemical shift). The conversion of the compound was determined with ^1H NMR.

Determination of enzyme kinetic parameters (Fig. 4)

To 200 μL of the substrate solution (7.5–80 mM for Ala-NH_2, 1.0–32 mM Ala-Gly, 0.60–15 mM Ala-Gly-NMe_2, 0.60–40 mM Ala-Gly-NHMe, 100 mM phosphate buffer, pH = 7.4, containing 0.5 mM valine for Ala-NH_2, Ala-Gly-NMe_2, and Ala-Gly-NHMe, or 0.5 mM threonine for Ala-Gly as internal standards) preincubated at 37 °C for 10 min was added a solution of recombinant human APN (1.62 nM, 200 μL, 100 mM phosphate buffer, pH = 7.4) preincubated at 37 °C for 10 min. The resulting solution was incubated at 37 °C and 100 μL was sampled at three time points (10, 20, and 30 min for Ala-NH_2, 2, 4, and 6 h for Ala-Gly, 5, 10, and 15 min for Ala-Gly-NMe_2, 20, 40, and 60 min for Ala-Gly-NHMe). The sampled solutions were added to 100 μL of the quenching solution (1.0 mM 1,10-phenanthroline, 5.0 mM EDTA, H_2O) and frozen with liquid nitrogen. The samples were kept on ice. After melting on ice, 10.0 μL of each sample was transferred to another vessel. To the vessel were added 80.0 μL of 50 mM borate buffer (pH = 8.0) containing 20 mM EDTA, and 20 μL of 100 mM NBD-F in MeCN, successively. After incubation at ambient temperature for 30 min and 60 °C for 3 min, the vessel was cooled on ice and then HCl aq. (50 mM, 20.0 μL) was added. The resulting solution was filtrated (Cosmonice Filter W®, 0.45 μm, Nacalai tesque) and analyzed with HPLC.

HPLC analysis

Elution was conducted with eluent A (H_2O containing 0.1% TFA) and eluent B (MeCN containing 0.1% TFA). Samples were analyzed with a linear gradient: 0–3.0 min, 18% B; 3.0–13 min, 18-20% B; 13–16 min, 20-99% B; 16–19 min, 99% B; 19–20 min, 99-18% B; 20–30 min, 18% B at a flow rate of 1.0 mL/min. HPLC charts were monitored at fluorescence intensity of 530 nm upon excitation at 470 nm. Ala in each sample was quantified with the ratio of NBD-Ala and NBD-Val or NBD-Thr.

Detection of APN-activity using Ala-[1-^{13}C]Gly-d_2-NMe_2 under thermal equilibrium state *for tissue homogenate*

The solution of 100 mM Ala-[1-^{13}C]Gly-d_2-NMe_2 (50.0 μL, 100 mM phosphate buffer, pH = 7.4) was added to the reaction solution containing tissue homogenate (30.0 μL), 100 mM phosphate buffer (365 μL), DMSO or 100 mM phebestin in DMSO (5.0 μL), and D_2O (50.0 μL). ^{13}C NMR was acquired (flip angle: 30°, relaxation delay: 2 s, 128 scans (*ca.* 7 min)) at 37 °C. DMSO was used as an internal standard (δ 39.04 ppm). Protein concentration of kidney homogenate was determined as 42 mg/mL with BCA assay (Thermo scientific). Tumor homogenate was prepared from the tumor xenograft (MIA PaCa-2) bearing mouse referring to our previous report (31).

for mouse serum

The solution of 100 mM Ala-[1-^{13}C]Gly-d_2-NMe_2 (60.0 μL, D_2O, pD = 7.4 adjusted with aqueous DCl) was added to the reaction solution containing mouse serum (540 μL). ^{13}C NMR was acquired (flip angle: 30°, relaxation delay: 2 s, 128 scans (*ca.* 7 min)) at 37 °C. The acquisition was repeated ten times.

8-5. Chemical shift and T_1 measurements under thermal equilibrium state (Fig. 3B, 3D and S13)

Chemical shift change in Fig. 3B was measured with a JEOL ECS400 (9.4 T). Measurement conditions: 100 mM each of the probe candidate and the product in phosphate buffer containing 10% D_2O (90 mM, pH = 7.4), 37 °C, pH was adjusted with 1 M NaOH aq.

The T_1 values under thermal equilibrium state in Figs. 3B and 3D and fig. S13 were measured with a JEOL ECS400 (9.4 T), JEOL ECA 500 (11.7 T), and JEOL ECA 600 (14.1 T) by the inversion recovery method. Representative measurement conditions (for Fig. 3B): 500 mM of the compound in phosphate buffer containing 10% D_2O (90 mM, pH = 7.4), 37 °C, 9.4 T, pH was adjusted with 35 wt% DCl in D_2O and 40 wt% NaOD in D_2O.

8-6. Hyperpolarization experiments

Preparation of the probe solution for hyperpolarization

Probe solution A

To 42.5 mg of Ala-[1-^{13}C]Gly-d_2-NMe_2 were added H_2O (22.2 μL), 10 M HCl aq. (9.4 μL), and OX063 (Oxford Instruments, UK) (1.1 mg). To the resulting mixture was added 12.6 μL of glycerol containing 19 mM OX063.

Probe solution B

To the vessel containing lyophilized Ala-[1-^{13}C]Gly-d_2-NMe_2 was added H_2O (173 nL/mg for Ala-[1-^{13}C]Gly-d_2-NMe_2). *Note: Ala-[1-^{13}C]Gly-d_2-NMe_2 is highly soluble into H_2O. The aqueous solution can be prepared with only a small amount of H_2O.* The highly viscous solution was neutralized with 10 M HCl aq. to pH *ca.* 7. The concentration of the probe typically became 4–5 M. To this solution was added OX063 (Oxford Instruments, UK, final concentration: 19 mM).

In vitro detection of APN activity under hyperpolarized state

for ^{13}C MR spectroscopy in vitro (Fig. 5C)

Probe solution A (25.0 μL) prepared above was hyperpolarized (dissolution buffer: 4.0 mL of DPBS containing 0.68 mM EDTA). To 2.0 mL of DPBS was added 1.0 mL of the hyperpolarized solution. Dynamic ^{13}C MR spectrum was acquired using a 3 T MRI scanner (repetition time = 1 s, flip angle = 10°). The apparent T_1 was obtained by curve fitting using the following eq. 3

$$I(t) = I(0)exp\left(\frac{-t}{T_1{}^{app}}\right) + y_0 \qquad (eq.3)$$

where I(t) is the signal intensity at an arbitrary time t; T_1^{app} is the apparent T_1; y_0 is the signal offset. The fitting algorithm was implemented in ImageJ. The corrected T_1 was obtained using the following eq. 4

$$\frac{1}{T_1{}^{corr}} = \frac{1}{T_1{}^{app}} + \ln(\cos\theta)\frac{1}{TR} \qquad (eq.4)$$

where T_1^{corr} is the corrected T_1; θ is the flip angle; TR is the repetition time.

for enzymatic reaction in vitro (Fig. 5D)

Probe solution A (23.0 μL) prepared above was hyperpolarized (dissolution buffer: 4.0 mL of DPBS containing 0.68 mM EDTA). To 3.0 mL of DPBS containing 250 nM rat APN (Merck 164599, Darmstadt, Germany) was added 1.2 mL of hyperpolarized solution. Dynamic ^{13}C MR spectrum was acquired using a 3 T MRI scanner (repetition time = 1 s, flip angle = 10°).

In vivo detection of APN activity in human pancreatic tumor xenograft bearing mouse *(Fig. 6, S10–S12)*

Probe solution B (40 or 80 μL for Figs. 6B, 6C, and fig. S10; 120 μL for Fig. 6G and figs S12A, and S12C; 80 μL for figs. S11, S12B, and S12D) prepared above was hyperpolarized (dissolution buffer: 4.0 mL of DPBS containing 0.68 mM EDTA). The hyperpolarized solution (*ca.* 400 μL) was injected into the tail vein of athymic nude mice bearing a tumor xenograft (MIA PaCa-2) in the hind leg. Dynamic ^{13}C MR spectrum was acquired using a 3 T MRI scanner using a 17 mm homebuilt ^{13}C solenoid coil placed inside of a ^{1}H saddle coil, which site-specifically detects a tumor region embedded in the right leg. The non-localized ^{13}C MRS were obtained with a spectral width of 3333 Hz, repetition time of 1 s, a flip angle of 10°. In this homebuilt ^{13}C solenoid coil area, approximately 75% of the tissue volume is attributed to tumor regions based on the analysis of the FLASH anatomical MRI scans, which have been addressed in our previous studies (57, 58). Anatomical images were acquired using a T_2-weighted fast spin-echo imaging sequence with a field of view of 28 mm × 28 mm with a 256 × 256 matrix, a 2 mm section thickness with a 2 mm intersection gap, a repetition time of 2500 ms, an effective echo time of 68 ms, an echo-train length of 8 echoes. All of the animal studies were approved by the National Cancer Institute Animal Care and Use Committee (NCI-CCR-ACUC) in accordance with the Guide for the Care and Use of Laboratory Animal Resources. *Note*: When the hyperpolarized solution is at a low magnetic field region close to the earth's magnetic field, the hyperpolarized signal will be reduced because of scalar relaxation by nearby ^{14}N nuclei. To avoid this problem, it is recommended to handle hyperpolarized solutions at a magnetic field strength above a certain level or to use a magnet for sample transfer (40, 59).

Administration of phebestin

The stock solution of phebestin (56.6 μL, 10 mM in DMSO) was dissolved into H_2O (43.4 μL). The diluted solution was intravenously injected into mice (10 mg/kg) 24 h after the measurement of APN-activity of the day 1.

REFERENCES AND NOTES

1. F. A. Howe, K. S. Opstad, ^{1}H MR spectroscopy of brain tumours and masses. *NMR Biomed.* **16**, 123–131 (2003).

2. B. Ross, A. Lin, K. Harris, P. Bhattacharya, B. Scweinsburg, Clinical experience with ^{13}C MRS *in vivo*. *NMR Biomed.* **16**, 358–369 (2003).

3. R. J. Gilles, D. L. Morse, In vivo magnetic resonance spectroscopy in cancer. *Annu. Rev. Biomed. Eng.* **7**, 287–326 (2005).

4. S. J. Kohut, M. J. Kaufman, Magnetic resonance spectroscopy studies of substance use disorders: Current landscape and potential future directions. *Pharmacol. Biochem. Behav.* **200**, 173090 (2021).

5. J. H. Ardenkjær-Larsen, B. Fridlund, A. Gram, G. Hansson, L. Hansson, M. H. Lerche, R. Servin, M. Thaning, K. Golman, Increase in signal-to-noise ratio of > 10,000 times in liquid-state NMR. *Proc. Natl. Acad. Sci. U.S.A.* **100**, 10158–10163 (2003).

6. K. Golman, René in ‘t Zandt, M. Thaning, Real-time metabolic imaging. *Proc. Natl. Acad. Sci. U.S.A.* **103**, 11270–11275 (2006).

7. S. J. Nelson, J. Kurhanewicz, D. B. Vigneron, P. E. Z. Larson, A. L. Harzstark, M. Ferrone, M. van Criekinge, J. W. Chang, R. Bok, I. Park, G. Reed, L. Carvajal, E. J. Small, P. Munster, V. K. Weinberg, J. H. Ardenkjær-Larsen, A. P. Chen, R. E. Hurd, L. I. Odegardstuen, F. J. Robb, J. Tropp, J. A. Murray, Metabolic imaging of patients with prostate cancer using hyperpolarized [1-^{13}C]pyruvate. *Sci. Transl. Med.* **5**, 198ra108 (2013).

8. K. R. Keshari, D. M. Wilson, Chemistry and biochemistry of ^{13}C hyperpolarized magnetic resonance using dynamic nuclear polarization. *Chem. Soc. Rev.* **43**, 1627–1659 (2014).

9. Y. Kondo, H. Nonaka, Y. Takakusagi, S. Sando, Design of nuclear magnetic resonance molecular probes for hyperpolarized bioimaging. *Angew. Chem. Int. Ed.* **60**, 14779–14799 (2021).

10. C. Mu, D. E. Korenchan, S. Wang, D. M. Wilson, R. R. Flavell, Tumor microenvironment biosensors for hyperpolarized carbon-13 magnetic resonance spectroscopy. *Mol. Imaging Biol.* **23**, 323–334 (2021).

11. N. J. Stewart, S. Matsumoto, Biomedical applications of the dynamic nuclear polarization and parahydrogen induced polarization techniques for hyperpolarized ^{13}C MR imaging. *Magn. Reson. Med. Sci.* **20**, 1–17 (2019).

12. S. Meier, P. R. Jensen, M. Karlsson, M. H. Lerche, Hyperpolarized NMR probes for biological assays. *Sensors* **14**, 1576–1597 (2014).

13. A. Comment, Dissolution DNP for *in vivo* preclinical studies. *J. Magn. Reson.* **264**, 39–48 (2016).

14. J. Kurhanewicz, D. B. Vigneron, J. H. Ardenkjær-Larsen, J. A. Bankson, K. Brindle, C. H. Cunningham, F. A. Gallagher, K. R. Keshari, A. Kjær, C. Laustsen, D. A. Mankoff, M. E. Merritt, S. J. Nelson, J. M. Pauly, P. Lee, S. Ronen, D. J. Tyler, S. S. Rajan, D. M. Spielman, L. Wald, X. L. Zhang, C. R. Malloy, R. Rizi, Hyperpolarized ^{13}C MRI: Path to clinical translation in oncology. *Neoplasia* **21**, 1–16 (2019).

15. Z. J. Wang, M. A. Ohliger, P. E. Z. Larson, J. W. Gordon, R. A. Bok, J. Slater, J. E. Villanueva-Meyer, C. P. Hess, J. Kurhanewicz, D. B. Vigneron, Hyperpolarized ^{13}C MRI: State of the art and future directions. *Radiology* **291**, 273–284 (2019).

16. L. M. Le Page, C. Guglielmetti, C. Taglang, M. M. Chaumeil, Imaging brain metabolism using hyperpolarized ^{13}C magnetic resonance spectroscopy. *Trends Neurosci.* **43**, 343–354 (2020).

17. T. Nishihara, H. A. I. Yoshihara, H. Nonaka, Y. Takakusagi, F. Hyodo, K. Ichikawa, E. Can, J. A. M. Bastiaansen, Y. Takado, A. Comment, S. Sando, Direct monitoring of γ-glutamyl transpeptidase activity in vivo using a hyperpolarized ^{13}C-labeled molecular probe. *Angew. Chem. Int. Ed.* **55**, 10626–10629 (2016).

18. P. R. Jensen, S. C. Serra, L. Miragoli, M. Karlsson, C. Cabella, L. Poggi, L. Venturi, F. Tedoldi, M. H. Lerche, Hyperpolarized [1,3-$^{13}C_2$] ethyl acetoacetate is a novel diagnostic metabolic marker of liver cancer. *Int. J. Cancer* **136**, E117–E126 (2015).

19. P. Mina-Osorio, The moonlighting enzyme CD13: Old and new functions to target. *Trends Mol. Med.* **14**, 361–371 (2008).

20. C. Y. Lu, M. A. Amin, D. A. Fox, CD13/aminopeptidase N is a potential therapeutic target for inflammatory disorders. *J. Immunol.* **204**, 3–11 (2020).

21. S. A. Amin, N. Adhikari, T. Jha, Design of aminopeptidase N inhibitors as anti-cancer agents. *J. Med. Chem.* **61**, 6468–6490 (2018).

22. J. Dixon, L. Kaklamanis, H. Turley, I. D. Hickson, R. D. Leek, A. L. Harris, K. C. Gatter, Expression of aminopeptidase-n (CD 13) in normal tissues and malignant neoplasms of epithelial and lymphoid origin. *J. Clin. Pathol.* **47**, 43–47 (1994).

23. L. Guzman-Rojas, R. Rangel, A. Salameh, J. K. Edwards, E. Dondossola, Y. G. Kim, A. Saghatelian, R. J. Giordano, M. G. Kolonin, F. I. Staquicini, E. Koivunen, R. L. Sidman, W. Arap, R. Pasqualini, Cooperative effects of aminopeptidase N (CD13) expressed by nonmalignant and cancer cells within the tumor microenvironment. *Proc. Natl. Acad. Sci. U.S.A.* **109**, 1637–1642 (2012).

24. K. Chen, W. H. Ma, G. Q. Li, J. Wang, W. D. Yang, L. P. Yap, L. D. Hughes, R. Park, P. S. Conti, Synthesis and evaluation of ^{64}Cu-labeled monomeric and dimeric NGR peptides for MicroPET imaging of CD13 receptor expression. *Mol. Pharm.* **10**, 417–427 (2013).

25. S. V. Bhagwat, J. Lahdenranta, R. Giordano, W. Arap, R. Pasqualini, L. H. Shapiro, CD13/APN is activated by angiogenic signals and is essential for capillary tube formation. *Blood* **97**, 652–659 (2001).

26. Y. H. Shao, W. S. Liang, F. Kang, W. D. Yang, X. W. Ma, G. Y. Li, S. Zong, K. Chen, J. Wang, A direct comparison of tumor angiogenesis with ^{68}Ga-labeled NGR and RGD peptides in HT-1080 tumor xenografts using microPET imaging. *Amino Acids* **46**, 2355–2364 (2014).

27. B. Delmas, J. Gelfi, R. Lharidon, L. K. Vogel, H. Sjostrom, O. Noren, H. Laude, Aminopeptidase N is a major receptor for the enteropathogenic coronavirus TGEV. *Nature* **357**, 417–420 (1992).

28. J. Li, L. Z. Chen, W. X. Wu, W. Zhang, Z. Ma, Y. N. Cheng, L. P. Du, M. Y. Li, Discovery of bioluminogenic probes for aminopeptidase N imaging. *Anal. Chem.* **86**, 2747–2751 (2014).

29. L. Z. Chen, W. Sun, J. Li, Z. Z. Liu, Z. Ma, W. Zhang, L. P. Du, W. F. Xu, H. Fang, M. Y. Li, The first ratiometric fluorescent probes for aminopeptidase N cell imaging. *Org. Biomol. Chem.* **11**, 378–382 (2013).

30. L. Z. Chen, W. Sun, W. H. Li, J. Li, L. P. Du, W. F. Xu, H. Fang, M. Y. Li, The first ratiometric fluorescent probe for aminopeptidase N. *Anal. Methods* **4**, 2661–2663 (2012).

31. R. Hata, H. Nonaka, Y. Takakusagi, K. Ichikawa, S. Sando, Design of a hyperpolarized molecular probe for detection of aminopeptidase N activity. *Angew. Chem. Int. Ed.* **55**, 1765–1768 (2016).

32. L. Chen, Y. L. Lin, G. Q. Peng, F. Li, Structural basis for multifunctional roles of mammalian aminopeptidase N. *Proc. Natl. Acad. Sci. U.S.A.* **109**, 17966–17971 (2012).

33. H. Nonaka, R. Hata, T. Doura, T. Nishihara, K. Kumagai, M. Akakabe, M. Tsuda, K. Ichikawa, S. Sando, A platform for designing hyperpolarized magnetic resonance chemical probes. *Nat. Commun.* **4**, 2441 (2013).

34. Y. Imakura, H. Nonaka, Y. Takakusagi, K. Ichikawa, N. R. Maptue, A. M. Funk, C. Khemtong, S. Sando, Rational design of [^{13}C,D_{14}] *tert*-butylbenzene as a scaffold structure for designing long-lived hyperpolarized ^{13}C probes. *Chem. Asian J.* **13**, 280–283 (2018).

35. E. D. Berker, R. R. Shoup, T. C. Farrar, ^{13}C NMR spectroscopy: Relaxation times of ^{13}C and methods for sensitivity enhancement. *Pure Appl. Chem.* **32**, 51–66 (1972).

36. C. Taglang, D. E. Korenchan, C. von Morze, J. Yu, C. Najac, S. N. Wang, J. E. Blecha, S. Subramaniam, R. Bok, H. F. VanBrocklin, D. B. Vigneron, S. M. Ronen, R. Sriram, J. Kurhanewicz, D. M. Wilson, R. R. Flavell, Late-stage deuteration of ^{13}C-enriched substrates for T_1 prolongation in hyperpolarized ^{13}C MRI. *Chem. Commun.* **54**, 5233–5236 (2018).

37. M. Nagai, F. Kojima, H. Naganawa, M. Hamada, T. Aoyagi, T. Takeuchi, Phebestin, a new inhibitor of aminopeptidase N, produced by *Streptomyces* sp. MJ716-m3. *J. Antibiot.* **50**, 82–84 (1997).

38. J. S. Blicharski, Nuclear magnetic relaxation by anisotropy of the chemical shift. *Z. Naturforsch.* **27A**, 1456–1458 (1972).

39. J. R. Brender, S. Kishimoto, G. R. Eaton, S. S. Eaton, Y. Saida, J. Mitchell, M. C. Krishna, Trehalose as an alternative to glycerol as a glassing agent for in vivo DNP MRI. *Magn. Reson. Med.* **85**, 42–48 (2021).

40. A. Cho, R. Eskandari, K. L. Granlund, K. R. Keshari, Hyperpolarized [6-^{13}C,$^{15}N_3$]-arginine as a probe for *in vivo* arginase activity. *ACS Chem. Biol.* **14**, 665–673 (2019).

41. J. R. Brender, S. Kishimoto, H. Merkle, G. Reed, R. E. Hurd, A. P. Chen, J. H. Ardenkjaer-Larsen, J. Munasinghe, K. Saito, T. Seki, N. Oshima, K. Yamamoto, P. L. Choyke, J. Mitchell, M. C. Krishna, Dynamic imaging of glucose and lactate metabolism by ^{13}C-MRS without hyperpolarization. *Sci. Rep.* **9**, 3410 (2019).

42. A. López-Perrote, R. Castaño, R. Melero, T. Zamarro, H. Kurosawa, T. Ohnishi, A. Uchiyama, K. Aoyagi, G. Buchwald, N. Kataoka, A. Yamashita, O. Llorca, Human nonsense-mediated mRNA decay factor UPF2 interacts directly with eRF3 and the SURF complex. *Nucleic Acids Res.* **44**, 1909–1923 (2016).

43. A. H. M. Wong, D. X. Zhou, J. M. Rini, The x-ray crystal structure of human aminopeptidase N reveals a novel dimer and the basis for peptide processing. *J. Biol. Chem.* **287**, 36804–36813 (2012).

44. T. D. Alger, W. D. Hamill Jr., R. J. Pugmire, D. M. Grant, G. D. Sllcox, M. Solum, Carbon-13 spin-lattice relaxation in condensed aromatic compounds. *J. Phys. Chem.* **84**, 632–636 (1980).

45. T. C. Wong, T. T. Ang, F. S. Guziec Jr., C. A. Moustakis, The chemical-shift anisotropy mechanism in ^{77}Se spin–lattice relaxation. measurement of ^{77}Se T_1 at several magnetic fields. *J. Magn. Reson.* **57**, 463–470 (1984).

46. B. R. Brooks, R. E. Bruccoleri, B. D. Olafson, D. J. States, S. Swaminathan, M. Karplus, CHARMM: A program for macromolecular energy, minimization, and dynamics calculations. *J. Comput. Chem.* **4**, 187–217 (1983).

47. D. Bashford, M. Karplus, p*K*a's of ionizable groups in proteins: Atomic detail from a continuum electrostatic model. *Biochemistry* **29**, 10219–10225 (1990).

48. Y. Nozaki, C. Tanford, Acid-base titrations in concentrated guanidine hydrochloride. Dissociation constants of the guamidinium ion and of some amino acids. *J. Am. Chem. Soc.* **89**, 736–742 (1967).

49. M. Tanokura, ^{1}H nuclear magnetic resonance titration curves and microenvironments of aromatic residues in bovine pancreatic ribonuclease A. *J. Biochem.* **94**, 51–62 (1983).

50. M. Tanokura, ^{1}H-NMR study on the tautomerism of the imidazole ring of histidine residues: I. Microscopic p*K* values and molar ratios of tautomers in histidine-containing peptides. *BBA-Protein Struc. M.* **742**, 576–585 (1983).

51. M. Tanokura, ^{1}H-NMR study on the tautomerism of the imidazole ring of histidine residues: II. Microenvironments of histidine-12 and histidine-119 of bovine pancreatic ribonuclease a. *BBA-Protein Struc. M.* **742**, 586–596 (1983).

52. B. Rabenstein, E.-W. Knapp, Calculated pH-dependent population and protonation of carbon-monoxy-myoglobin conformers. *Biophys. J.* **80**, 1141–1150 (2001).

53. QSite, version 5.8, Schrödinger, LLC, New York, NY, 2012.

54. W. L. Jorgensen, D. S. Maxwell, J. Tirado-Rives, Development and testing of the OPLS all-atom force field on conformational energetics and properties of organic liquids. *J. Am. Chem. Soc.* **118**, 11225–11236 (1996).

55. Molecular Operating Environment (MOE), 2018.0101; (Chemical Computing Group Inc. Montreal, Canada, 2018).

56. A. Eguchi, M. Nakakido, S. Nagatoishi, D. Kuroda, K. Tsumoto, T. Nagamune, M. Kawahara, An epitope-directed antibody affinity maturation system utilizing mammalian cell survival as readout. *Biotechnol. Bioeng.* **116**, 1742–1751 (2019).

57. S. Matsumoto, S. Kishimoto, K. Saito, Y. Takakusagi, J. P. Munasinghe, N. Devasahayam, C. P. Hart, R. J. Gillies, J. B. Mitchell, M. C. Krishna, Metabolic and physiologic imaging biomarkers of the tumor microenvironment predict treatment outcome with radiation or a hypoxia-activated prodrug in mice. *Cancer Res.* **78**, 3783–3792 (2018).

58. N. Oshima, R. Ishida, S. Kishimoto, K. Beebe, J. R. Brender, K. Yamamoto, D. Urban, G. Rai, M. S. Johnson, G. Benavides, G. L. Squadrito, D. Crooks, J. Jackson, A. Joshi, B. T. Mott, J. H. Shrimp, M. A. Moses, M.-J. Lee, A. Yuno, T. D. Lee, X. Hu, T. Anderson, D. Kusewitt, H. H. Hethaway, A. Jadhav, D. Picard, J. B. Trepel, J. B. Mitchell, G. M. Stott, W. Moore, A. Simeonov, L. A. Sklar, J. P. Norenberg, W. M. Linehan, D. J. Maloney, C. V. Dang, A. G. Waterson, M. Hall, V. M. Darley-Usmar, M. C. Krishna, L. M. Neckers, Dynamic imaging of LDH inhibition in tumors reveals rapid *In Vivo* metabolic rewiring and vulnerability to combination therapy. *Cell Rep.* **30**, 1798–1810.e4 (2020).

59. E. Chiavazza, E. Kubala, C. V. Gringeri, S. Düwel, M. Durst, R. F. Schulte, M. I. Menzel, Earth's magnetic field enabled scalar coupling relaxation of ^{13}C nuclei bound to fast-relaxing quadrupolar ^{14}N in amide groups. *J. Magn. Reson.* **227**, 35–38 (2013).